Mineralogical Magazine, 2015, Vol. 79(2), pp. 309–319

Crystallographic ordering of aluminium in laueite at Hagendorf-Süd

I. E. Grey[1,*], E. Keck[2], W. G. Mumme[1], C. M. MacRae[1], J. R. Price[3], A. M. Glenn[1] and C. J. Davidson[1]

[1] CSIRO Mineral Resources, Private Bag 10, Clayton South, Victoria 3169, Australia
[2] Algunderweg 3, 92694 Etzenricht, Germany
[3] Australian Synchrotron, 800 Blackburn Road, Clayton, Victoria 3168, Australia

[*Received 28 May 2014; Accepted 15 August, 2014; Associate Editor: S. J. Mills*]

ABSTRACT

Crystals of laueite, $Mn^{2+}Fe_2^{3+}(PO_4)_2(OH)_2{\cdot}8H_2O$, from the Cornelia mine open cut, Hagendorf Süd, Bavaria, are zoned due to aluminium incorporation at the iron sites, with analysed Al_2O_3 contents varying up to 11 wt.%. Synchrotron X-ray data were collected on two crystals with different Al contents and the structures refined. The laueite structure contains two independent Fe^{3+}-containing sites; *M*2 and *M*3, which alternate in 7 Å corner-connected octahedral chains. The coordination polyhedra are different for the two sites, $M2O_4(OH)_2$ and $M3O_2(OH)_2(H_2O)_2$ respectively. The structure refinements show that Al preferentially orders into site *M*3. Refined site occupancies for *M*2 and *M*3 for the two crystals are: for crystal L-1, *M*2 = 0.70(1) Fe + 0.30(1) Al, *M*3 = 0.54(1) Fe + 0.46(1) Al and for crystal L-2, *M*2 = 0.67(1) Fe + 0.33(1) Al, *M*3 = 0.48(1) Fe + 0.52(1) Al. For crystal L-2, the octahedral chains have dominant Fe in *M*2, alternating with dominant Al in *M*3 along the chain, an ordering phenomenon not previously reported for laueite-related minerals.

Keywords: ordering, aluminium, laueite, Hagendorf-Süd, Germany.

Introduction

The phosphate zones within the Hagendorf Süd granitic pegmatites in Bavaria have provided a rich source of phosphate minerals for both researchers and collectors, from the late 19th century to the close of mining and natural flooding of the deposit in 1984. Of the more than 180 minerals identified at the Cornelia mine within the Hagendorf-Süd pegmatite, 85 are phosphates, including 12 for which Hagendorf Süd is the type locality (Yakovenchuk *et al*., 2012). The primary and metasomatically exchanged primary phosphates at Hagendorf include arrojadite, $KNa_4CaMn_4Fe_{10}Al(PO_4)_{12}(OH,F)_2$, fluorapatite, graftonite, $(Fe,Mn,Ca)_3(PO_4)_2$, hagendorfite, $(Na,Ca,Mn)_2MnFe_2(PO_4)_3$, sarcopside, $(Fe,Mn,Mg)_3(PO_4)_2$, scorzalite, $(Fe,Mg)Al_2(PO_4)_2(OH)_2$, triphyllite, $Li(Fe,Mn)PO_4$, the triplite-zwieselite series, $(Fe,Mn)_2PO_4(F,OH)$ and wolfeite, $FeMn(PO_4)OH$ (Yakovenchuk *et al*., 2012). As described in detail for pegmatitic phosphates (e.g. Moore, 1973; Mücke, 1981; Shigley and Brown, 1985; Dill *et al*., 2008) these primary phosphates undergo hydrothermal replacement reactions, leaching and oxidation to produce a remarkable diversity of secondary phosphate minerals. The majority of secondary phosphates are hydrous Fe–Mn phosphates and basic phosphates with either Fe or Mn dominant in different crystallographic sites and with different ratios of divalent to trivalent Fe and Mn. Extra complexity comes from incorporation of additional elements from contacting fluids. At Hagendorf, Zn, UO_2, Ca, F and Al are important in this regard (Mücke, 1981).

Much of the diversity in secondary phosphate minerals comes from ordering of divalent cations in particular crystallographic sites. For example, eleven different whiteite–jahnsite minerals,

* E-mail: ian.grey@csiro.au
DOI: 10.1180/minmag.2015.079.2.09

$XM1M2_2M2_2^{3+}(PO_4)_4(OH)_2{\cdot}8H_2O$ (M^{3+} = Al^{3+}/Fe^{3+} for whiteite/jahnsite), have been approved by the International Mineralogical Association Commission on New Minerals and Nomenclature (IMA-CNMNC) based on different dominant divalent cations Ca^{2+}, Fe^{2+}, Mn^{2+} and Mg^{2+} in the three sites *X*, *M*1 and *M*2. Whiteite-(CaMnMn) is the most recent type mineral from the Hagendorf-Süd deposit (Yakovenchuk *et al.*, 2012). Similarly in the laueite-group minerals, $M^{2+}M2_2^{3+}(PO_4)_2(OH)_2{\cdot}8H_2O$, M^{3+} = Al^{3+} or Fe^{3+}, a number of species have been characterized based on different dominant divalent elements in the M^{2+} site (Krivovichev, 2004). Extensive solid-solution mixing of different divalent cations at the same site is common in such minerals (Moore and Ito, 1978; Grey *et al.*, 2010; Yakovenchuk *et al.*, 2012).

In contrast to extensive divalent cation mixing, solid solutions between species with different trivalent cations Fe^{3+} and Al^{3+} in phosphate minerals are rarely reported. With respect to whiteite–jahnsite minerals, Moore and Ito (1978) noted that "there is no evidence as yet that solid solution between the two is extensive". Recent studies, however, have identified compositional zoning in both whiteite–jahnsite and laueite–paravauxite occurrences at the Palermo #2 pegmatite, New Hampshire (Nizamoff, 2006) and in whiteite–jahnsite phases at Hagendorf Süd (Grey *et al.*, 2010; Yakovenchuk *et al.*, 2012). Quite extensive Al^{3+}/Fe^{3+} solid-solution ranges were found for whiteite–jahnsite. Moreover, there are two independent M^{3+} sites in these minerals and crystal-structure refinements of Fe-bearing whiteite-(CaMnMn) by two research groups agree that Fe^{3+} preferentially orders into one of the two Al^{3+} sites (Grey *et al.*, 2010; Yakovenchuk *et al.*, 2012).

Studies on Al^{3+}/Fe^{3+} mixing in pegmatitic secondary phosphate minerals can provide valuable information on the reaction conditions that prevailed and on likely precursor phases in the pegmatite. For example, in our recent study on Al-bearing strunzite $(Mn,Fe)^{2+}(Fe,Al)_2^{3+}(PO_4)_2(OH)_2{\cdot}6H_2O$, from the Cornelia mine, Hagendorf Süd, the quantification of Al incorporation at the Fe^{3+} sites provided key information for the development of a paragenesis mechanism whereby strunzite formed from Al-bearing jahnsite by selective leaching of divalent cation phosphate layers (Grey *et al.*, 2012). In this present paper we report the extension of these studies to the case of Al incorporation in laueite, $Mn^{2+}Fe_2^{3+}(PO_4)_2(OH)_2{\cdot}8H_2O$, at Hagendorf Süd.

Experimental

Sample

A hand specimen containing Al-bearing laueite in a small cavity on altered zwieselite was collected by EK from the 67 m level of the Cornelia mine open cut. The mineral forms sprays or rounded aggregates of very thin, often deformed, yellow laths. The morphology and colour of the laueite is so similar to those for other laueite-related polymorphs and jahnsite that X-ray studies are essential for correct identification (Moore and Araki, 1974). It is possible that some previously reported stewartite occurrences at Hagendorf Süd (Mücke, 1981) are in fact Al-bearing laueite. Associated minerals are Al-bearing beraunite, frondellite and jahnsite-(CaMnMn).

Analyses

A portion of the cavity rim was excised and mounted in an epoxy block, polished and carbon-coated for scanning electron microscopy (SEM) examination and electron microprobe (EMP) analyses. The analyses were conducted using wavelength dispersive spectrometry on a JEOL JXA 8500F Hyperprobe operated at an accelerating voltage of 12 kV and a beam current of 1 nA. The beam was defocused to 5 μm. Standards used were $CaSiO_3$ for Ca; $AlPO_4$ for Al, P; $MgAl_2O_4$ for Mg; hematite for Fe; $MnSiO_3$ for Mn; and ZnS for Zn. The EMP results are given in Table 1. All EMP data were corrected using a Phi–Rho–Z matrix correction (Armstrong, 1988).

Crystal fragments that were separated from the laueite grains for synchrotron XRD studies were checked for their Al content using standardless energy-dispersive X-ray analysis. The crystals were mounted on double-sided conducting tape fitted to a metal sample holder. Care was taken to ensure that the largest flat surfaces of the crystals were uppermost and horizontal. The energy dispersive spectra (EDS) were obtained using an FEI Quanta 400 field emission environmental SEM.

Synchrotron X-ray data collections and structure refinements

Six laueite laths, with compositions shown by EDS to span the range from lowest to highest Al content, were checked on the macromolecular beam line MX2 of the Australian Synchrotron. It

https://doi.org/10.1180/minmag.2015.079.2.09 Published online by Cambridge University Press

TABLE 1. Electron microprobe analyses (wt.%) for Al-bearing laueite from Hagendorf-Süd.

	Average (of 10 analyses)	Range	Calculated for laueite
Fe as Fe_2O_3	29.5	23.4–33.3	29.9
MnO	9.21	7.15–11.6	13.3
MgO	1.21	0.73–1.64	–
ZnO	1.24	0–2.46	–
Al_2O_3	8.00	1.79–11.1	–
P_2O_5	30.8	28.4–32.5	26.6
H_2O			30.2
Total	79.9	69.7–84.8	100.0

was found that the diffracting quality was inversely related to the Al content. With increasing Al content the mosaicity and appearance of split reflections increased markedly. Only the two crystals with the lowest Al contents gave diffraction data that could be indexed by the MX2 software. These two crystals, labelled L-1 and L-2, were used for synchrotron X-ray data collections. Data were collected at 298 K using an ADSC Quantum 315r detector and monochromatic radiation with a wavelength of 0.7100 Å. A phi scan was employed with a framewidth of 1º and a counting time per frame of 1 s. The intensity data sets were processed using *XDS* software to produce data files which were analysed in *WinGX* (Farrugia, 1999). The refinements were made using *SHELXL-97* (Sheldrick, 2008).

The two laueite datasets were indexed by the *XDS* software in triclinic cells with $a \approx 5.35$, $b \approx 7.2$, $c \approx 10.35$ Å, $\alpha \approx 97.1$, $\beta \approx 101.1$, $\gamma \approx 111.5$º. After application of the matrix (1 0 0, 1 0 1, 0 1 0) to transform the cells to those reported for laueite-group minerals (Krivovichev, 2004) the atomic coordinates for ushkovite (Galliski and Hawthorne, 2002) were used as starting coordinates for refinements in $P\bar{1}$. The EMP analyses had confirmed that the laueite crystals had dominant Mn in the divalent site, together with minor Fe, Zn and Mg. The scattering curve for Mn was used to represent Mn/Fe/Zn and the occupancies of Mn and Mg were refined for this site. The Al/Fe occupancies were refined in the two trivalent cation sites. As EMP analyses consistently gave an excess of metal atoms, typically 3.2*M* to 2P, difference Fourier maps were scanned for evidence of extra metal atoms, without success. An alternative possibility is a deficiency of P. Refinement of the *P* site occupancy reduced the *R* factor, with a *P* site occupancy of 0.95–0.96 for both crystals.

Difference Fourier maps revealed the positions of all hydroxyl and water H atoms. Following Kampf *et al*. (2014) the O–H distances were restrained to be 0.95(2) Å and the H–H distances for the water molecules were restrained to be 1.45(3) Å. For the lower-Al crystal L-1, individual H isotropic displacement parameters were refined, whereas for the more disordered L-2 crystal an overall isotropic displacement parameter was employed for the H atoms. Refinement of anisotropic displacement parameters for all non-H atoms gave the agreement factors reported in Table 2. The refined atomic coordinates, equivalent isotropic displacement parameters and site occupancies are given in Table 3. Tables of anisotropic displacement parameters and observed and calculated structure factors have been deposited with the Principal Editor of *Mineralogical Magazine* and are available from www.minersoc.org/pages/e_journals/dep_mat_mm.html.

Results and discussion

SEM and EMP analysis results

The laueite crystals were found to be extremely sensitive to the effects of vacuum and the electron beam. Prolonged high-vacuum pumping prior to carbon coating of samples for analyses resulted in the propagation of cracks throughout the crystals, with resultant plucking out of crystal fragments from the sample block. After analyses the yellow colour of the crystals was observed to have been completely bleached, leaving silvery white crystals. Adjacent yellow jahnsite crystals were not affected in this way. The EMP totals for laueite

https://doi.org/10.1180/minmag.2015.079.2.09 Published online by Cambridge University Press

TABLE 2. Data collection and structure refinement details for Al-bearing laueite crystals.

	Crystal L-1	Crystal L-2
Formula, from average EMP	$Mn_{0.55}Fe_{0.25}Mg_{0.13}Zn_{0.07}[Fe_{2-x}Al_x](PO_4)_{1.85}(OH)_2{\cdot}8(H_2O,OH)$	
x, from site occupancy factor refinement	0.76	0.86
Crystal data		
Cell parameters		
a, b, c (Å)	5.374(1), 10.717(3), 7.200(1)	5.320(5), 10.670(5), 7.139(5)
α, β, γ (°)	107.60(3), 111.52(3), 71.65(2)	107.71(1), 111.405(5), 71.84(8)
Volume (Å^3)	357.8(1)	350.1(4)
Z	2	2
Space group	$P\bar{1}$	$P\bar{1}$
Calculated density (g cm^{-1})	2.34	2.38
Data collection		
Temperature (K)	293	293
Wavelength (Å)	0.7100	0.7100
Crystal size (mm)	0.08 × 0.06 × 0.01	0.06 × 0.03 × 0.01
Collection mode	Phi scan, 360°, ΔΦ = 1°	Phi scan, 360°, ΔΦ = 1°
Count time per frame (s)	1	1
$2\theta_{max}$ (°)	52.7	52.7
No. of unique reflections	1331	1249
No. of reflections, $I > 2\sigma(I)$	1294	1162
R_{int}	0.059	0.060
Absorption coefficient (mm^{-1})	2.46	2.43
Multiscan T_{min}, T_{max}	0.55, 0.75	0.61, 0.75
Refinement		
Data/restraints/parameters	1331/0/155	1249/0/146
Goodness-of-fit	1.144	1.115
Final R indices ($F > 4\sigma(F)$)	R_1 =0.037, wR_2 = 0.095	R_1 =0.051, wR_2 = 0.155
Final R indices (all data)	R_1 =0.038, wR_2 = 0.095	R_1 =0.054, wR_2 = 0.156
Largest diff. peak and hole (e/Å^3)	+0.49, −0.58	+0.57. −0.95

were typically ~80%, whereas, based on the water content in laueite, the oxide totals should only be ~70%. Evidently water is lost during the evacuation and analyses (Kampf *et al.*, 2014). Loss of coordinated water could account for the observed colour change.

A backscattered electron (BSE) image of Al-bearing laueite and associated minerals is shown in Fig. 1. The laueite is most closely associated with sprays of green Al-bearing beraunite needles. The EMP analyses of the beraunite gave an average composition $Fe_{5.5}Al_{0.4}Mn_{0.1}(PO_4)_4(OH)_5{\cdot}6H_2O$. Refinement of synchrotron X-ray data on a beraunite needle showed that the Al was preferentially ordered in one crystallographic site, $M(2)$ (see Moore and Kampf (1992) for site notation), but the amount was not large enough (40% Al + 60% Fe) to

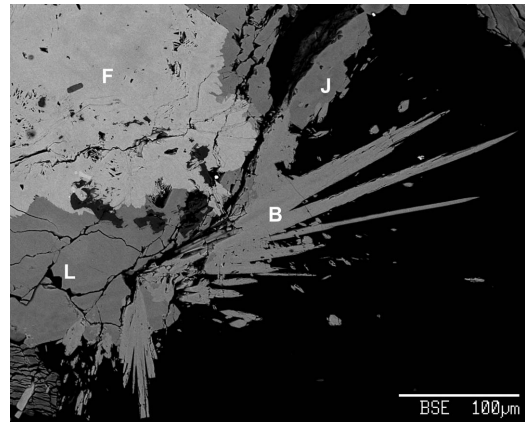

FIG. 1. Backscattered electron image showing Al-bearing laueite (L) and associated minerals, beraunite (B), frondelite (F) and jahnsite (J).

https://doi.org/10.1180/minmag.2015.079.2.09 Published online by Cambridge University Press

TABLE 3. (*a*) Refined coordinates, site occupancies and equivalent isotropic displacement parameters for Al-bearing laueite crystal L-1 (lower Al).

Atom	Site occupancy factors	*x*	*y*	*z*	U_{eq}
*M*1	0.85(1)Mn + 0.15(1)Mg	0	0	0	0.0127(3)
*M*2	0.70(1)Fe + 0.30(1)Al	0	0.5	0	0.0098(3)
*M*3	0.54(1)Fe + 0.46(1)Al	0	0.5	0.5	0.0091(3)
P1	0.961(6)	0.34520(15)	0.66917(7)	0.92610(12)	0.0113(3)
O1		0.1660(4)	0.6539(2)	0.0417(3)	0.0155(5)
O2		0.3010(4)	0.5749(2)	0.7112(3)	0.0163(5)
O3		0.2702(4)	0.8168(2)	0.9039(4)	0.0160(5)
O4		0.3448(4)	0.3678(2)	0.9510(3)	0.0154(5)
O5		0.1530(5)	0.5047(2)	0.2969(3)	0.0159(5)
O6		0.2346(5)	0.3109(2)	0.5435(4)	0.0178(5)
O7		0.2404(5)	0.0064(3)	0.3215(4)	0.0245(6)
O8		0.2284(5)	0.1107(2)	0.9465(4)	0.0235(6)
O9		0.2684(5)	0.8015(3)	0.5087(4)	0.0215(6)
H1		0.334(4)	0.493(4)	0.323(7)	0.026(11)
H2		0.290(8)	0.317(5)	0.680(3)	0.032(12)
H3		0.396(6)	0.275(5)	0.512(6)	0.036(12)
H4		0.239(11)	0.083(3)	0.422(6)	0.049(15)
H5		0.217(14)	−0.055(4)	0.374(8)	0.072(19)
H6		0.121(8)	0.193(3)	0.974(9)	0.055(16)
H7		0.398(5)	0.119(5)	0.974(8)	0.040(13)
H8		0.252(13)	0.810(6)	0.633(4)	0.061(18)
H9		0.180(9)	0.740(4)	0.422(6)	0.048(14)

Table 3. (*b*) Refined coordinates, site occupancies and equivalent isotropic displacement parameters for Al-bearing laueite crystal L-2 (higher Al).

Atom	Site occupancy factors	*x*	*y*	*z*	U_{eq}
*M*1	0.82(1)Mn +0.18(1)Mg	0	0	0	0.0247(5)
*M*2	0.67(1)Fe + 0.33(1)Al	0	0.5	0	0.0185(4)
*M*3	0.48(1)Fe + 0.52(1)Al	0	0.5	0.5	0.0196(4)
P1	0.959(7)	0.34423(17)	0.66927(9)	0.92645(13)	0.0191(5)
O1	O	0.1675(5)	0.6529(3)	0.0436(4)	0.0245(7)
O2	O	0.2965(5)	0.5769(3)	0.7102(4)	0.0258(7)
O3	O	0.2704(5)	0.8167(3)	0.9082(4)	0.0281(7)
O4	O	0.3454(5)	0.3676(3)	0.9528(4)	0.0248(7)
O5	O	0.1525(5)	0.5039(3)	0.2973(4)	0.0271(7)
O6	O	0.2344(6)	0.3141(3)	0.5445(4)	0.0300(7)
O7	O	0.2394(8)	0.0072(4)	0.3238(6)	0.0503(9)
O8	O	0.2273(6)	0.1104(4)	0.9461(7)	0.0490(10)
O9	O	0.2657(7)	0.8026(4)	0.5071(5)	0.0425(9)
H1	H	0.337(5)	0.489(8)	0.329(11)	0.092(9)
H2	H	0.295(14)	0.329(8)	0.684(3)	0.092(9)
H3	H	0.383(10)	0.264(7)	0.503(9)	0.092(9)
H4	H	0.183(17)	0.090(3)	0.400(9)	0.092(9)
H5	H	0.234(17)	−0.052(5)	0.391(10)	0.092(9)
H6	H	0.123(11)	0.195(3)	0.971(11)	0.092(9)
H7	H	0.403(6)	0.119(7)	0.987(11)	0.092(9)
H8	H	0.253(17)	0.800(7)	0.630(5)	0.092(9)
H9	H	0.191(15)	0.734(5)	0.418(8)	0.092(9)

https://doi.org/10.1180/minmag.2015.079.2.09 Published online by Cambridge University Press

qualify as a new mineral. High levels of Al have been reported in beraunite from the Krasno ore district, Czech Republic, by Sejkora *et al*. (2006). Other minerals associated with laueite in Fig. 1 are jahnsite and frondelite. An analysis of jahnsite gave a composition $Ca_{1.0}Mn_{2.2}Fe_{2.5}Mg_{0.2}Al_{0.1}(PO_4)_4(OH)_2{\cdot}8H_2O$, confirming it as jahnsite-(CaMnMn). Jahnsite-(CaMnMn) has been identified previously associated with nordgauite, $MnAl_2(PO_4)_2(F,OH)_2{\cdot}5.5H_2O$ (Birch *et al.*, 2011) and zwieselite–triplite (*senso stricto*) at Hagendorf Süd (Grey *et al.*, 2010). Analysis of the frondelite also showed it to be Al bearing, with an average composition from EMP analyses of $Fe_{4.1}Mn_{0.8}Al_{0.1}(PO_4)_3(OH)_5$.

High-contrast BSE images coupled with EMP analyses of laueite grains show them to be compositionally zoned due to variation in Al/Fe. A BSE image of a zoned laueite grain is shown in Fig. 2. Enrichment of Al occurs around the edges of the grain, and the boundaries between high-Al and low-Al zones are sharp. Another feature of the laueite grains is fine-scale cracking and separation into thin laths as shown in Fig. 2. The laths are parallel to (0 1 0). The parallel cracking shown in Fig. 2 was evident in low-vacuum studies on uncoated samples and is different from the random cracking induced by strong vacuum pumping. The textural features shown in Fig. 2, with topochemical enrichment of Al, a sharp reaction interface and extensive cracking are characteristic of mineral-replacement reactions, which take place primarily by leaching–reprecipitation processes (Putnis, 2002). The fine-scale cracking and associated misalignment of adjacent crystallites with increasing Al incorporation results in a significant decrease in diffraction quality, which limited our structural studies to the lower levels of Al enrichment.

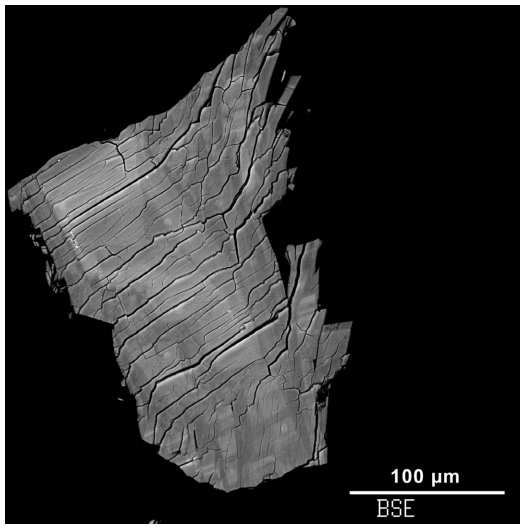

FIG. 2. Backscattered electron image showing zoning due to Al/Fe variations in Al-bearing laueite.

The EMP analyses of laueite crystals are given in Table 1. The Al_2O_3 contents range from <2 wt.% in the cores of the grains to over 11 wt.% in the rims. An atomic plot of [Al] *vs.* [Fe] gives a moderate negative correlation with $R^2 = 0.67$. The compositions obtained from the analyses, scaled to $2(PO_4)$ are metal rich with $\Sigma M \approx 3.2$. There is a weak positive correlation ($R^2 = 0.33$) between the metal excess and Al content. We tried, without success, to find evidence for extra metal atoms in difference Fourier maps during the single-crystal structure refinements. An alternative interpretation, that the mineral is deficient in phosphate, was supported by *P* site occupation refinement. A possible explanation, consistent with the positive correlation with Al content, is that PO_4 is partially replaced by CO_3, as can occur in the Al-phosphate minerals crandallite and plumbogummite (Grey *et al*., 2011).

Based on full octahedral metal-atom site occupancy, the empirical composition from the average of the EMP analyses is $[Mn_{0.55}Fe_{0.25}Mg_{0.13}Zn_{0.07}]^{2+}[Fe_{1.33}Al_{0.67}]^{3+}(PO_4)_{1.85}(OH)_2{\cdot}8(H_2O,OH)$. The lowest and highest Al contents of the crystals analysed gave calculated compositions of $[Mn_{0.71}Mg_{0.12}\ Zn_{0.11}Fe_{0.06}]^{2+}[Fe_{1.84}Al_{0.16}]^{3+}(PO_4)_{1.95}(OH)_2{\cdot}8(H_2O,OH)$ and $[Mn_{0.52}Mg_{0.16}Zn_{0.06}Fe_{0.26}]^{2+}[Fe_{1.03}Al_{0.97}]^{3+}(PO_4)_2(OH)_2{\cdot}8H_2O$.

Crystal structure results

Refinement results for the two Al-bearing laueite crystals, L-1 and L-2, are given in Tables 3*a* and 3*b*, while polyhedral bond lengths and water molecule geometries are reported in Table 4. The bond distances associated with the interlayer *M*1 atom are very similar to those reported for mangangordonite (Leavens and Rheingold, 1988) and kastningite (Adiwidjaja *et al*., 1999), which both have dominant Mn and minor Fe in the *M*1 site. The average bond lengths associated with the octahedral atoms *M*2 and *M*3 are shorter than reported for ushkovite (Galliski and

https://doi.org/10.1180/minmag.2015.079.2.09 Published online by Cambridge University Press

TABLE 4. Polyhedral bond lengths and water molecule geometries for Al-bearing laueite crystals from Hagendorf-Süd.

	Crystal L-1 (lower Al)	Crystal L-2 (higher Al)
*M*1–O3 (×2)	2.136(2)	2.116(3)
–O8 (×2)	2.145(3)	2.122(4)
–O7 (×2)	2.190(3)	2.185(4)
Average	2.157	2.141
*M*2–O5 (×2)	1.980(2)	1.968(3)
–O1 (×2)	2.009(2)	1.988(3)
–O4 (×2)	2.022(2)	2.007(3)
Average	2.004	1.988
*M*3–O5 (×2)	1.941(2)	1.915(3)
–O2 (×2)	1.961(2)	1.935(3)
–O6 (×2)	2.069(2)	2.035(3)
Average	1.990	1.962
P–O3	1.547(2)	1.532(3)
–O2	1.551(2)	1.537(3)
–O1	1.554(2)	1.542(3)
–O4	1.559(2)	1.545(3)
Average	1.553	1.539
O6–H2	0.90(2)	0.91(2)
–H3	0.91(2)	0.90(2)
H2–O6–H3	102.5(2.8)º	105.4(3.6)º
O7–H4	0.92(2)	0.91(2)
–H5	0.91(2)	0.92(2)
H4–O7–H5	104.1(3.2)º	104.2(3.5)º
O8–H6	0.90(2)	0.90(2)
–H7	0.89(2)	0.90(2)
H6–O8–H7	108.4(3.2)º	105.4(3.6)º
O9–H8	0.90(2)	0.91(2)
–H9	0.89(2)	0.90(2)
H8–O9–H9	107.4(3.4)º	103.6(3.5)º

Hawthorne, 2002) and stewartite (Moore and Araki, 1974), reflecting the partial Al incorporation. The H-atom positions found in difference Fourier maps agree with those reported for ushkovite by Galliski and Hawthorne (2002). The H-bonding scheme for crystal L-1 is reported in Table 5.

The structure of lauite, as well as that of numerous related minerals and synthetic phases (Krivovichev, 2004), is essentially a sheet structure, based on the sheet motif shown in Fig. 3. The sheets are parallel to (0 1 0) and comprise butlerite-like (Fanfani and Zanazzi, 1971) 7 Å kinked chains of *trans*-corner-connected octahedra parallel to the *c* axis, decorated with corner-connected PO_4 tetrahedra. Two types of octahedra alternate along the chain, with coordination polyhedra $M2O_4(OH)_2$ and $M3O_2(OH)_2(H_2O)_2$. Adjacent chains link by corner-connection between the octahedra and tetrahedra as shown in Fig. 3 to form (0 1 0) sheets of composition $M2M3(PO_4)_2(OH)_2(H_2O)_2$. The linkage of the *M*2-centred octahedra and the PO_4 tetrahedra gives rise to kröhnkite-like (Hawthorne, 1985) 5.3 Å chains parallel to the *a* axis.

The (0 1 0) sheets are connected along *b* by corner-connection of the PO_4 tetrahedra with $M1O_2(H_2O)_4$ octahedra as shown in Fig. 4. In isostructural laueite-group minerals this site is occupied by divalent cations, Mn^{2+}, Mg^{2+} or Fe^{2+} (Krivovichev, 2004 and references therein). There is also an oxidized form, named sigloite (Hurlbut and Honea, 1962; Hawthorne, 1988), with Fe^{3+} in the *M*1 site. The phosphate mineral curetonite Ba(Al,Ti)(PO_4)(O,OH)F (Cooper and Hawthorne, 1994) and a number of synthetic phases such as $(enH_2)Fe_2F_2(HPO_4)_2(H_2O)_2$, en = ethylenediamine (Cavellec *et al*., 1994) and $(enH_2)NbFeOF(PO_4)_2(H_2O)_2$ (Wang *et al*. 2000) have topologically identical laueite-type sheets but different connectivity to species between the sheets. Stewartite (Moore and Araki, 1974) and kastningite (Adiwidjaja *et al*., 1999) have sheets that differ in the orientation of the PO_4 groups, up or down, relative to the plane of the sheet, and are described as geometric isomers (Moore, 1970, 1975; Krivovichev, 2004). The phosphates pseudolaueite (Baur, 1969), metavauxite (Baur and Rao, 1967) and strunzite (Fanfani *et al.*, 1978) have similar sheets but a topologically different connectivity between the octahedra and tetrahedra and are called topological isomers, while geometrical isomerism further separates the first from the latter two minerals (Krivovichev, 2004).

The most interesting new aspect of laueite-group minerals, obtained in this study, is the preferential ordering of Al in one of the trivalent metal-atom sites, *M*3 at (0,½,½). As seen from the site-occupancy refinements in Table 3, the crystal containing smaller amounts of Al, L-1, has 30(1)% Al in the *M*2 site and 46(1) Al in the *M*3 site, while the crystal containing larger amounts of Al, L-2, has 33(1)% Al in *M*2 and 52(1)% Al in *M*3. The overall larger Al content of

https://doi.org/10.1180/minmag.2015.079.2.09 Published online by Cambridge University Press

TABLE 5. Hydrogen bonds for laueite crystal L-1.

D–H···A	D–H	H···A	D···A	<DHA
O5–H1···O2	0.89(2)	1.95(2)	2.804(3)	160(4)
O6–H2···O4	0.90(2)	1.80(2)	2.684(3)	167(4)
O6–H3···O9	0.91(2)	1.77(2)	2.676(3)	171(4)
O7–H4···O6	0.92(2)	2.33(3)	3.166(4)	151(4)
O7–H5···O9	0.91(2)	1.95(3)	2.846(4)	166(6)
O8–H6···O1	0.90(2)	1.87(3)	2.739(3)	164(5)
O8–H7···O3	0.89(2)	1.92(2)	2.776(3)	162(4)
O9–H8···O3	0.90(2)	1.90(2)	2.797(4)	172(6)
O9–H9···O5	0.89(2)	2.44(3)	3.231(3)	149(4)

crystal L-2 was confirmed from EDS analyses on the crystals, giving 6.0 wt.% Al_2O_3, compared with 4.1 wt.% Al_2O_3 for L-1. The higher Al content of the *M*3 site is reflected in the shorter bond lengths as shown in Table 4. Although ordering of different cations in the two sites *M*2 and *M*3 has not been reported for laueite-group minerals, it is known for synthetic phases containing laueite-type sheets. In $(enH_2)Fe_2F_2(HPO_4)_2(H_2O)_2$ (Cavellec *et al*., 1994) Fe^{3+} is ordered in *M*2 and Fe^{2+} in *M*3. In $(enH_2)NbFeOF(PO_4)_2(H_2O)_2$ (Wang *et al*. 2000) Nb^{5+} occupies *M*2 and Fe^{3+} occupies *M*3 and in $(enH_2)Ti(Fe,Cr)(F,O)(H_{0.3}PO_4)_2(H_2O)_2$ (Wang *et al*. 2000), Ti^{4+} occupies *M*2 and Fe^{3+}/Cr^{3+} occupies *M*3.

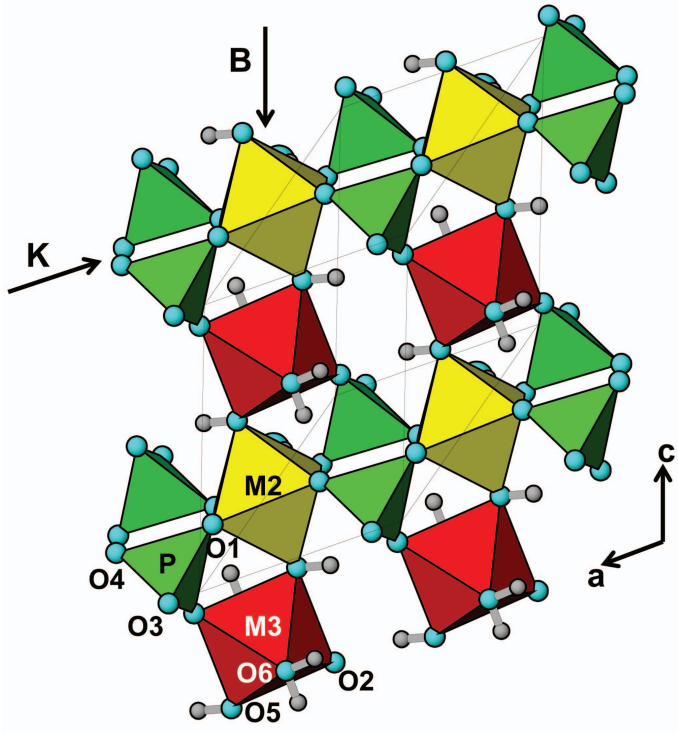

FIG. 3.The heteropolyhedral (0 1 0) sheet in laueite. Butlerite-type (B) and kröhnkite-type (K) chains are indicated by arrows.

https://doi.org/10.1180/minmag.2015.079.2.09 Published online by Cambridge University Press

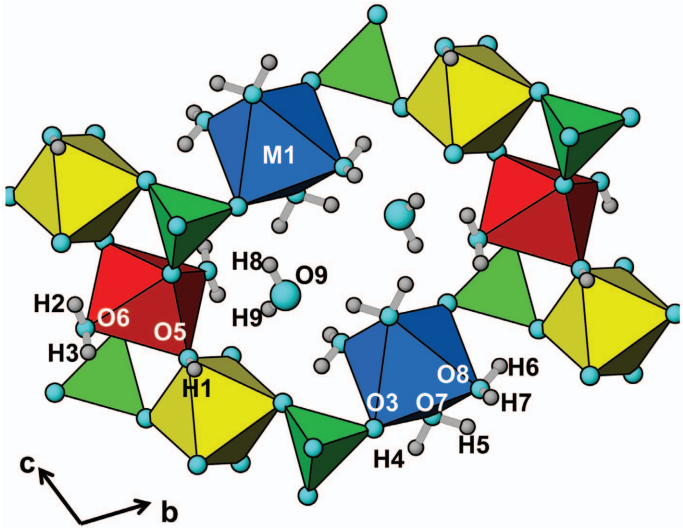

FIG. 4. Connectivity between the laueite heteropolyhedral sheets, *via* $M1O_2(H_2O)_4$ octahedra, viewed along [1 0 0]. The OH, coordinated OH_2 and H_2O bonds are labelled.

In each of these phases the higher-valence cation has coordination $M2O_4(F,O)_2$ and the lower-valence cation has coordination $M3O_2(F,O)_2(H_2O)_2$. In the phosphate minerals that are different topological isomers to laueite (pseudolaueite, metavauxite and strunzite), the two trivalent metal atoms have the same coordination, $MO_4OH(H_2O)$. The sites are equivalent in pseudolaueite and metavauxite but independent in strunzite. A recent refinement of Al-bearing strunzite from Hagendorf Süd (Grey *et al*., 2012) shows no preferential ordering of Al, with 0.28(1) Al + 0.72(1) Fe in the two independent sites This suggests that the ordering found in Al-bearing laueite is related to the different anion coordination of the two sites.

In the synthetic phases, as well as in laueite-group minerals, the *M*3 site is the larger of the two so it is perhaps surprising that the smaller cation, Al^{3+}, is preferentially ordered into this site, with Fe^{3+} dominant in the *M2* site. This may be related to the mechanism of formation of the mineral. If Al was incorporated into pre-existing laueite by a mineral-replacement reaction, then the *M*3 site with the weaker bonds to surrounding anions would be the more likely site for replacement.

The topology and geometrical isomerism of minerals that have equivalent heteropolyhedral sheets to laueite have been discussed in detail by Krivovichev (2004). Since the Krivovichev publication, three new laueite-group minerals have been reported; ferrolaueite, $Fe^{2+}Fe_2^{3+}(PO_4)_2(OH)_2{\cdot}8H_2O$ (Segeler *et al*., 2012), maghrebite, $MgAl_2(AsO_4)_2(OH)_2{\cdot}8H_2O$ (Meisser *et al*., 2012) and césarferreiraite, $Fe^{2+}Fe_2^{3+}(AsO_4)_2(OH)_2{\cdot}8H_2O$ (Scholz *et al*., 2014). The presence of both arsenate and phosphate minerals with either Al or Fe dominant in the sites *M*2 and *M*3 prompted a review of nomenclature for the minerals and a nomenclature proposal for the laueite supergroup has been approved by the IMA-CNMNC, voting proposal 14-F (http://pubsites.uws.edu.au/ima-cnmnc/). The structure-refinement data for crystal L-2 confirms that it is built from laueite sheets, but with different dominant atoms, Fe and Al, in the two crystallographically independent trivalent cation sites, *M*2 and *M*3, respectively. This mineral will require approval from the IMA to qualify as a new mineral of the laueite supergroup.

Acknowledgements

The authors acknowledge access to the Macromolecular beam line MX2 at the Australian Synchrotron, for collection of single-crystal X-ray data.

References

Adiwidjaja, G., Friese, K., Klaska, K.-H. and Schlüter, J. (1999) The crystal structure of kastningite

https://doi.org/10.1180/minmag.2015.079.2.09 Published online by Cambridge University Press

$(Mn,Fe,Mg)(H_2O)_4[Al_2(OH)_2(H_2O)_2(PO_4)_2]\cdot 2H_2O$ – a new hydroxyl aquated orthophosphate hydrate mineral. *Zeitschrift für Kristallographie*, **214**, 465–468.

Armstrong, J.T. (1988) Quantitative analysis of silicate and oxide materials: comparison of Monte Carlo, ZAF and Phi–Rho–Z procedures. *Microbeam Analysis*, 239–246.

Baur, W.H. (1969) A comparison of the crystal structures of pseudolaueite and laueite. *American Mineralogist*, **54**, 1312–1323.

Baur, W.H. and Rao, B.R. (1967) The crystal structure of metavauxite. *Naturwissenschaften*, **54**, 561.

Birch, W.D., Grey, I.E., Mills, S.J., Pring, A. Wilson, N.C. and Keck, E. (2011) Nordgauite, $MnAl_2(PO_4)_2(F,OH)_2.5.5H_2O$, a new mineral from the Hagendorf Süd pegmatite, Bavaria, Germany: description and crystal structure. *Mineralogical Magazine*, **75**, 269–278.

Cavellec, M., Riou, D. and Ferey, G. (1994) Oxyfluorinated microporous compounds. XI. Synthesis and crystal structure of ULM-10: The first bidimensional mixed-valence iron fluorophosphates with intercalated ethylenediamine. *Journal of Solid State Chemistry*, **112**, 441–447.

Cooper, M. and Hawthorne, F.C. (1994) The crystal structure of curetonite, a complex heteropolyhedral sheet mineral. *American Mineralogist*, **79**, 545–549.

Dill, H.G., Weber, B., Gerdes, A. and Melcher, F. (2008) The Fe-Mn phosphate aplite 'Silbergrube' near Waidhaus, Germany: epithermal phosphate mineralization in the Hagendorf-Pleystein province. *Mineralogical Magazine*, **72**, 1119–1144.

Fanfani, I. and Zanazzi, P.F. (1971) The crystal structure of butlerite. *American Mineralogist*, **56**, 751–757.

Fanfani, L., Tomassini, M., Zanazzi, P.F. and Zanzari, A.R. (1978) The crystal structure of strunzite, a contribution to the crystal chemistry of basic ferric-manganous hydrated phosphates. *Tschermaks Mineralogische und Petrographische Mitteilungen*, **25**, 77–87.

Farrugia, L.J. (1999) WinGX suite for small-molecule single-crystal crystallography. *Journal of Applied Crystallography*, **32**, 837–838.

Galliski, M.A. and Hawthorne, F.C. (2002) Refinement of the crystal structure of ushkovite from Nevados de Palermo, Republica Argentina. *The Canadian Mineralogist*, **40**, 929–937.

Grey, I.E., Mumme, W.G., Neville, S.M., Wilson, N.C. and Birch, W.D. (2010) Jahnsite–whiteite solid solutions and associated minerals in the phosphate pegmatite at Hagendorf-Süd, Bavaria, Germany. *Mineralogical Magazine*, **74**, 969–978.

Grey, I.E., Shanks, F.L., Wilson, N.C., Mumme, W.G. and Birch, W.D. (2011) Carbon incorporation in plumbogummite-group minerals. *Mineralogical Magazine*, **75**, 145–158.

Grey, I.E., MacRae, C.M., Keck, E. and Birch, W.D. (2012) Aluminium-bearing strunzite derived from Jahnsite at the Hagendorf-Süd pegmatite, Germany. *Mineralogical Magazine*, **76**, 1165–1174.

Hawthorne, F.C. (1985) Towards a structural classification of minerals: The $^{VI}M^{IV}T_2\Phi_n$ minerals. *American Mineralogist*, **70**, 455–473.

Hawthorne, F.C. (1988) Sigloite: The oxidation mechanism in $[M_2^{3+}(PO_4)_2(OH)_2(H_2O)_2]^{2-}$ structures. *Mineralogy and Petrology*, **38**, 201–211.

Hurlbut, C.S. and Honea, R. (1962) Sigloite, a new mineral from Llallagua, Bolivia. *American Mineralogist*, **47**, 1–8.

Kampf, A.R., Hughes, J.M., Nash, B. and Marty, J. (2014) Kokinosite, $Na_2Ca_2(V_{10}O_{26})\cdot 24H_2O$, a new decavanadate mineral species from the St. Jude mine, Colorado: crystal structure and descriptive mineralogy. *The Canadian Mineralogist*, **52**, 15–25.

Krivovichev, S.V. (2004) Topological and geometrical isomerism in minerals and inorganic compounds with laueite-type heteropolyhedral sheets. *Neues Jahrbuch für Mineralogie Monatshafte*, **2004**, 209–220.

Leavens, P.B. and Rheingold, A.L. (1988) Crystal structures of gordonite, $MgAl_2(PO_4)_2(OH)_2(H_2O)_6(H_2O)_2$, and its Mn analog. *Neues Jahrbuch für Mineralogie Monatshafte*, **1988**, 265–270.

Meisser, N., Brugger, J., Krivovichev, S., Armbruster, T. and Favreau, G. (2012) Description and crystal structure of maghrebite, $MgAl_2(AsO_4)_2(OH)_2\cdot 8H_2O$, from Aghbar, Anti-Atlas, Morocco: first arsenate in the laueite mineral group. *European Journal of Mineralogy*, **24**, 717–726.

Moore, P.B. (1970) Structural hierarchies among minerals containing octahedrally coordinating oxygen. I. Stereoisomerism among corner-sharing octahedral and tetrahedral chains. *Neues Jahrbuch für Mineralogie Monatshafte*, **1970**, 163–173.

Moore, P.B. (1973) Pegmatite phosphates: Descriptive mineralogy and crystal chemistry. *The Mineralogical Record*, **4**, 103–130.

Moore, P.B. (1975) Laueite, pseudolaueite, stewartite and metavauxite: A study in combinatorial polymorphism. *Neues Jahrbuch für Mineralogie Abhandlugen*, **1975**, 148–159.

Moore, P.B. and Araki, T. (1974) Stewartite, $Mn^{2+}Fe_2^{3+}(OH)_2(H_2O)_6[PO_4]_3\cdot 2H_2O$: Its atomic arrangement. *American Mineralogist*, **59**, 1272–1276.

Moore, P.B. and Ito, J. (1978) I. Whiteite, a new species, and a proposed nomenclature for the jahnsite-whiteite complex series, II. New data on xanthoxenite. III. Salmonsite discredited. *Mineralogical Magazine*, **42**, 309–323.

Moore, P.B. and Kampf, A.R. (1992) Beraunite: Refinement, comparative crystal chemistry, and

https://doi.org/10.1180/minmag.2015.079.2.09 Published online by Cambridge University Press

selected bond valences. *Zeitschrift für Kristallographie*, **201**, 263–281.

Mücke, A. (1981) The paragenesis of the phosphate minerals of the Hagendorf pegmatite – a general view. *Chemie der Erde*, **40**, 217–234.

Nizamoff, J. (2006) *The mineralogy, geochemistry and phosphate paragenesis of the Palermo #2 pegmatite, North Groton, New Hampshire*. MSc Thesis, University of New Orleans, USA.

Putnis, A. (2000) Mineral replacement reactions: From macroscopic observations to microscopic mechanisms. *Mineralogical Magazine*, **66**, 689–708.

Scholz, R., Chukanov, N.V., Menezes Filho, L.A.D., Attencio, D., Lagoeiro, L., Belotti, F.M., Chaves, M.L.S.C., Romano, A.W., Brandao, P.R., Belakovskiy, D.I. and Pekov, I. (2014) Césarferreiraite, $Fe^{2+}Fe_2^{3+}(AsO_4)_2(OH)_2{\cdot}8H_2O$, from Eduardo mine, Conselheiro Pena, Minas Gerais, Brazil: Second arsenate in the laueite mineral group. *American Mineralogist*, **99**, 607–611.

Segeler, C.G., Moore, P.B. Dyar, M.D., Leans, F. and Ferraiolo, J.A. (2012) Ferrolaueite, a new mineral from Monmouth County, New Jersey, USA, *Australian Journal of Mineralogy*, **16**, 69–76.

Sejkora, J., Skoda, R., Ondrus, P., Beran, P. and Süsser, C. (2006) Mineralogy of phosphate accumulations in the Huber stock, Krasno ore district, Slavkovsky les area, Czech Republic. *Journal of the Czech Geological Society*, **51**, 103–147.

Sheldrick, G.M. (2008) A short history of SHELX. *Acta Crystallographica*, **A64**, 112–122.

Shigley, J.E. and Brown, G.E. (1985) Occurrence and alteration of phosphate minerals at the Stewart Pegmatite, Pala District, San Diego County, California. *American Mineralogist*, **70**, 395–408.

Wang, X., Liu, L., Cheng, H., Ross, K. and Jacobson, A.J. (2000) Synthesis and crystal structures of $[H_3N(CH_2)_2NH_3]NbMOF(PO_4)_2(H_2O)_2$, M = Fe, Co and $[H_3N(CH_2)_2NH_3]Ti(Fe_{0.9}Cr_{0.1})(F_{1.3}O_{0.7})(H_{0.3}PO_4)_2(H_2O)_2$. *Journal of Materials Chemistry*, **10**, 1203–1208.

Yakovenchuk, V.N., Keck, E., Krivovichev, S.V., Pakhomovsky, Y.A., Selivanova, E.A., Mikhailova, J.A., Chernyatieva, A.P. and Ivanyuk, G.Yu. (2012) Whiteite-(CaMnMn), $CaMnMn_2Al_2[PO_4]_4(OH)_2{\cdot}8H_2O$, a new mineral from the Hagendorf-Süd granitic pegmatite, Germany. *Mineralogical Magazine*, **76**, 2761–2771.

https://doi.org/10.1180/minmag.2015.079.2.09 Published online by Cambridge University Press